






RESEARCH ARTICLE

10.1029/2023AV000877

The Influence of Convective Aggregation on the Stable Isotopic Composition of Water Vapor

Peer Review The peer review history for this article is available as a PDF in the Supporting Information.

Joseph Galewsky¹ , Matthias Schneider², Christopher Diekmann^{2,3}, Addisu Semie^{4,5} , Sandrine Bony⁵, Camille Risi⁵, Kerry Emanuel⁶, and Helene Brogniez⁷ 

Key Points:

- Remote sensing datasets are used to study the impact of convective aggregation on the atmospheric hydrologic cycle in the global tropics
- Unaggregated convection is associated with top-heavy ascent profiles, increased mixing ratios, and decreased water vapor isotopic ratios
- Aggregated convection is associated with bottom-heavy ascent profiles and positive correlation with mixing ratio and vapor isotopic ratios

Supporting Information:

Supporting Information may be found in the online version of this article.

Correspondence to:

J. Galewsky,
galewsky@unm.edu

Citation:

Galewsky, J., Schneider, M., Diekmann, C., Semie, A., Bony, S., Risi, C., et al. (2023). The influence of convective aggregation on the stable isotopic composition of water vapor. *AGU Advances*, 4, e2023AV000877. <https://doi.org/10.1029/2023AV000877>

Received 11 JAN 2023
Accepted 13 AUG 2023

Author Contributions:

Conceptualization: Joseph Galewsky, Sandrine Bony, Camille Risi, Kerry Emanuel

Formal analysis: Joseph Galewsky, Matthias Schneider, Christopher Diekmann, Kerry Emanuel

Funding acquisition: Joseph Galewsky, Matthias Schneider

¹Department of Earth and Planetary Sciences, University of New Mexico, Albuquerque, NM, USA, ²Institute of Meteorology and Climate Research (IMK-ASF), Karlsruhe Institute of Technology, Karlsruhe, Germany, ³Now at Software Solutions Department, Telespazio Germany GmbH, Darmstadt, Germany, ⁴Computational Data Science Program, Addis Ababa University, Addis Ababa, Ethiopia, ⁵LMD/IPSL, Sorbonne University, CNRS, Paris, France, ⁶Lorenz Center, Massachusetts Institute of Technology, Cambridge, MA, USA, ⁷Laboratoire Atmosphères, Milieux, Observations Spatiales (LATMOS/IPSL, UVSQ Université Paris-Saclay, Sorbonne Université, CNRS), Guyancourt, France

Abstract Remote sensing datasets of water vapor isotopic composition are used along with objective measures of convective aggregation to better understand the impact of convective aggregation on the atmospheric hydrologic cycle in the global tropics (30°N to 30°S) for the period 2015–2020. When convection is unaggregated, vertical velocity profiles are top-heavy, mixing ratios increase and water vapor δD decreases as the mean precipitation rate increases, consistent with partial hydrometeor evaporation below anvils into a relatively humid atmospheric column. Aggregated convection is associated with bottom-heavy vertical velocity profiles and a positive correlation between mixing ratio and δD , a result that is consistent with isotopic enrichment from detrainment of shallow convection near the observation level. Intermediate degrees of aggregation do not display significant variation in δD with mixing ratio or precipitation rate. Convective aggregation provides a useful paradigm for understanding the relationships between mixing ratio and isotopic composition across a range of convective settings. The results presented here may have utility for a variety of applications including the interpretation of paleoclimate archives and the evaluation of numerical simulations of convection.

Plain Language Summary Convective clouds in the atmosphere can aggregate in a variety of ways, from individual cells to larger systems like tropical cyclones and squall lines. Some recent studies have examined how the aggregation of clouds affects water vapor, which can have an impact on the Earth's climate. In this study, we use remote sensing measurements of water vapor isotopic composition along with objective measurements of cloud organization to understand how the convective aggregation affects the water cycle in the tropics from 2015 to 2020. When clouds are not aggregated, there is more moisture in the atmosphere and water vapor becomes more isotopically depleted with increasing rain rates, while aggregated clouds are associated with less moisture and isotopic enrichment of water vapor with increasing rain rates. These findings could be useful for understanding past climates and for evaluating computer simulations of clouds and climate.

1. Introduction

Convective clouds exhibit a wide range of organizational styles, from randomly scattered convective cells to mesoscale convective systems and tropical cyclones (Holloway et al., 2017). Numerical modeling studies with increasingly high resolution have yielded important insights into the processes that govern the organization or aggregation of convective clouds (Bretherton et al., 2005; Held et al., 1993; Muller & Held, 2012), and have shown that aggregation is favored by a combination of surface flux, moisture, and radiative feedbacks (Wing et al., 2017). Several recent studies have explored how the insights from modeling studies may be applied to understanding the influence of convective aggregation on the climate of the tropics (Bony et al., 2020; Semie & Bony, 2020) and how convective aggregation influences humidity (Tobin et al., 2012; Wing et al., 2017). In particular, unaggregated convection is often associated with a moister atmosphere, a large extent of upper-tropospheric clouds, and a top-heavy ascent profile, while aggregated convection is more commonly associated with a drier atmosphere, little upper-tropospheric cloud cover, and a bottom-heavy ascent profile (Tsai & Mapes, 2022). Such variations in humidity have impacts on outgoing longwave radiation, with important implications for climate (Bony et al., 2020).

© 2023. The Authors.

This is an open access article under the terms of the [Creative Commons Attribution-NonCommercial-NoDerivs License](https://creativecommons.org/licenses/by-nc-nd/4.0/), which permits use and distribution in any medium, provided the original work is properly cited, the use is non-commercial and no modifications or adaptations are made.

Investigation: Joseph Galewsky, Kerry Emanuel

Methodology: Joseph Galewsky, Matthias Schneider, Christopher Diekmann, Addisu Semie, Sandrine Bony, Camille Risi, Kerry Emanuel, Helene Brogniez

Project Administration: Joseph Galewsky

Resources: Joseph Galewsky

Software: Addisu Semie

Supervision: Kerry Emanuel

Validation: Matthias Schneider, Christopher Diekmann, Addisu Semie, Camille Risi

Visualization: Joseph Galewsky, Addisu Semie, Kerry Emanuel

Writing – original draft: Joseph Galewsky, Matthias Schneider, Sandrine Bony, Camille Risi, Kerry Emanuel, Helene Brogniez

Writing – review & editing: Joseph Galewsky, Matthias Schneider, Christopher Diekmann, Addisu Semie, Sandrine Bony, Camille Risi, Kerry Emanuel, Helene Brogniez

While modeling studies provide important clues about the influence of convective aggregation on humidity, extending these insights to observations can be more challenging owing to the difficulty of diagnosing the range of processes that control humidity. The stable isotopic composition of atmospheric water vapor, expressed with δ notation as defined below, is a sensitive recorder of phase changes of water substance and mixing between different airmasses (Craig, 1961; Galewsky et al., 2016; Noone, 2012). The isotopic composition of water vapor in an air parcel reflects its history of phase changes and mixing with other air parcels. Whenever there is a phase change, heavier isotopologues preferentially remain in the condensed phase. The evaporation of condensate can influence the stable isotopic composition of water vapor through the partial evaporation of isotopically light water from hydrometeors (Lawrence et al., 2004; Lee & Fung, 2008; Risi et al., 2021). Mixing between water vapor in different airmasses yields a resulting isotopic composition that is a humidity-weighted combination of the different airmasses that are mixed (Galewsky & Hurley, 2010). Diluting (mixing) a moist airmass with a much drier airmass has only a weak impact on the isotopic composition of the mixture (Risi et al., 2019). In such a case, the mixture will have a lower overall mixing ratio (q) but the isotopic composition of the water vapor will overwhelmingly reflect the isotopic composition of the moister airmass owing to the much greater water vapor abundance in the moist airmass. To the extent that convective aggregation affects the humidity of the environment around convection, stable isotopic measurements may thus provide a useful pathway for improved understanding of how convective aggregation influences humidity.

Worden et al. (2007) showed a negative correlation between free tropospheric δD and q over large geographic regions of the tropics using satellite data and attributed this relationship to rain evaporation processes. Lacour et al. (2018) explored the impact of the depth of convection and precipitation intensity on the isotopic composition of mid-tropospheric water vapor. They showed how shallow convection can isotopically enrich the middle troposphere through the convective detrainment of boundary layer air; in contrast, deep convection can isotopically deplete the middle troposphere through partial hydrometeor evaporation into relatively humid air as the lighter isotopologues preferentially evaporate, and through downdrafts of isotopically depleted water vapor. In the former case, latent heating is observed to peak in the lower atmosphere, while latent heating peaks in the upper troposphere for deeper convection. In general, the mixing ratio is correlated with water vapor δ values, meaning that more humid air parcels tend to be more isotopically enriched. This positive correlation can be attributed to mixing of isotopically-enriched boundary layer air into the free troposphere by convection. In cases of top-heavy large-scale ascent, however, q and δ are anti-correlated. Lacour et al. (2018) found that anti-correlated $q - \delta$ pairs are associated with deep convection and hydrometeor evaporation from above, although they also suggested that convective downdrafts could play a role in this anti-correlation. Torri et al. (2017) showed that different structures of vertical velocities are associated with different isotopic abundances and that precipitation in the eastern part of the Pacific is more enriched than in the western part, implying that velocity profiles in the East are more bottom heavy than in the West Pacific. Hurley et al. (2019) linked the changing slope of the $\delta D - q$ relationship during different phases of the Madden-Julian Oscillation to transitions in convection from shallow (with detrainment) to deep (with rain evaporation). Similar results were found by Diekmann, Schneider, Knippertz, et al. (2021), who found that different combinations of air mass mixing, Rayleigh condensation during convection, and microphysical processes that deplete the vapor determine the final isotopic composition in the Sahelian troposphere during the monsoon. While these studies did not explicitly focus on convective aggregation, their results, along with previous studies that have indicated systematic links between aggregation and humidity, suggest that there should be a coherent link between convective aggregation and the isotopic composition of water vapor. This is the hypothesis we test here.

This study is facilitated by two key recent advances. First is our ability to quantitatively measure the state of convective aggregation from observations. A quantitative metric for the degree of aggregation is essential for a thorough analysis, and several approaches have been developed in recent years, each of which focuses on particular characteristics of aggregated convection. Some of these methods include the Simple Convective Aggregation Index (SCAI) of Tobin et al. (2012), which is based on the numbers of convective clusters within a region along with the average distances between clusters; the subsidence fraction method of Coppin and Bony (2015); an approach based on the spatial variance of moist static energy (Wing & Emanuel, 2014); the convective organization potential (COP) of White et al. (2017); the morphological index of convective aggregation (Kadoya & Masunaga, 2018); the area-based convective organization potential method of Jin et al. (2022), and the shape-based BLW method of Beucler et al. (2020). Tompkins and Semie (2017) developed the I_{org} index for use in numerical models, based on statistical comparisons with a pure random process. This method was extended to observations

by Semie and Bony (2020) who used minima in infrared brightness temperatures to identify convective clusters. We use the I_{org} metric in this study, although similar results are obtained using SCAI or the number of convective clusters in a domain. The other key advance is the global, multi-year MUSICA IASI data set of paired H_2O and δD (Diekmann, Schneider, Ertl, et al., 2021). This data set provides twice-daily global observations, giving us an unprecedented window into the global isotopic composition of atmospheric water vapor. In this study, we take advantage of these advances to elucidate the links between convective aggregation, humidity, and the stable isotopic composition of water vapor.

2. Methods and Data Sets

We report the isotopic composition of water vapor in permil (‰), relative to Vienna Standard Mean Ocean Water using δ notation (e.g., $\delta D = (R/R_{VSMOW} - 1) \times 1,000$, where R is the D/H ratio). The starting point for understanding the covariability of mixing ratio (q) and isotopic composition (δ) in the atmosphere is the idealized process of Rayleigh distillation, during which water vapor in an ascending air parcel condenses and fractionates such that heavier isotopologues of water preferentially move into the condensate, leaving the remaining vapor depleted in the heavier isotopologues. The ratio R_r of heavy to light isotope in the vapor reservoir is described by:

$$R_r = R_o f^{\alpha-1} \quad (1)$$

where R_o is the initial isotopic ratio of the vapor, f is the fraction of original vapor remaining, and α is the fractionation factor between phases. This process leads to a change in the isotopic composition of both the precipitation that forms and the remaining water vapor as heavier isotopologues preferentially fractionate into the condensed phase. Further details on Rayleigh distillation and its implications may be found in Galewsky et al. (2016).

The relationships between water vapor mixing ratio and its isotopic composition can be visualized on a $q - \delta$ diagram. Such diagrams serve as the foundation of many studies of water vapor isotopic composition (Noone, 2012; Samuels-Crow et al., 2014; Worden et al., 2007). Within this framework, the Rayleigh curve can be considered a reference process. As described in previous studies (Galewsky, 2018a, 2018b) the difference, in permil, between an isotopic measurement at a given mixing ratio and the δ -value of the idealized Rayleigh distillation process to the same mixing ratio is a useful metric that can be interpreted in terms of moistening and mixing processes. This quantity will be referred to here as D_{rl} . This metric is similar to the δD_q used by Bailey et al. (2017). A high, or more positive, value of D_{rl} occurs when an isotopic value lies above a Rayleigh curve and is interpreted as representing a small degree of moistening of a dry, isotopically-depleted airmass by a moist, isotopically-enriched airmass (Galewsky & Hurley, 2010), while low or negative of D_{rl} are interpreted as representing greater evaporative moistening. This latter process is sometimes referred to as “super-Rayleigh” (Noone, 2012).

For this study, we computed the mixing ratios and δD values for Rayleigh distillation along a pseudoadiabatic lapse rate computed from averaged ERA reanalysis between 30°N and 30°S from the 2015–2020 period. The starting isotopic composition was computed using the closure assumption of Merlivat and Jouzel (1979). With an average SST over the tropical domain of 299.5 K, 2 m air temperature of 298.1 K, 2 m Relative humidity (RH) of 77.5%, we calculated a starting water vapor δD of -72.6 ‰ and a lifted condensation level of 940 hPa.

We characterize the spatial organization of convective clusters using the I_{org} index of Tompkins and Semie (2017) and Semie and Bony (2020), which is computed using 3-hourly inter-calibrated infrared brightness temperature (T_b) from GridSat-B1 (Knapp et al., 2011) between 30°N and 30°S every 1° in a moving $10^\circ \times 10^\circ$ box, for a total of 14,400 domains within the tropics. For each 3-hourly snapshot of T_b , we identify deep convective centroids as the points of local minima in the T_b field. Once the convective centroids are identified, the distances between nearest-neighbor (NN) centroids are calculated. The I_{org} index compares the cumulative density function of the calculated NN distances (NNCDF) with that expected from a random distribution of the same number of convective centroids. For a random distribution associated with a Poisson process, the cumulative density function (PNNCDF) is given by a Weibull function as:

$$PNNCDF = 1 - \exp(-\lambda \pi r^2) \quad (2)$$

where λ is the number of convective centroids per unit area and r is the nearest-neighbor distance. Values of I_{org} that are larger than 0.5 correspond to a clustered distribution of deep convective clouds, while $I_{org} = 0.5$ represents randomly distributed convection. Further details on this method are provided in Tompkins and Semie (2017) and Semie and Bony (2020). The 3-hourly I_{org} data is interpolated in time and space to each MUSICA IASI retrieval.

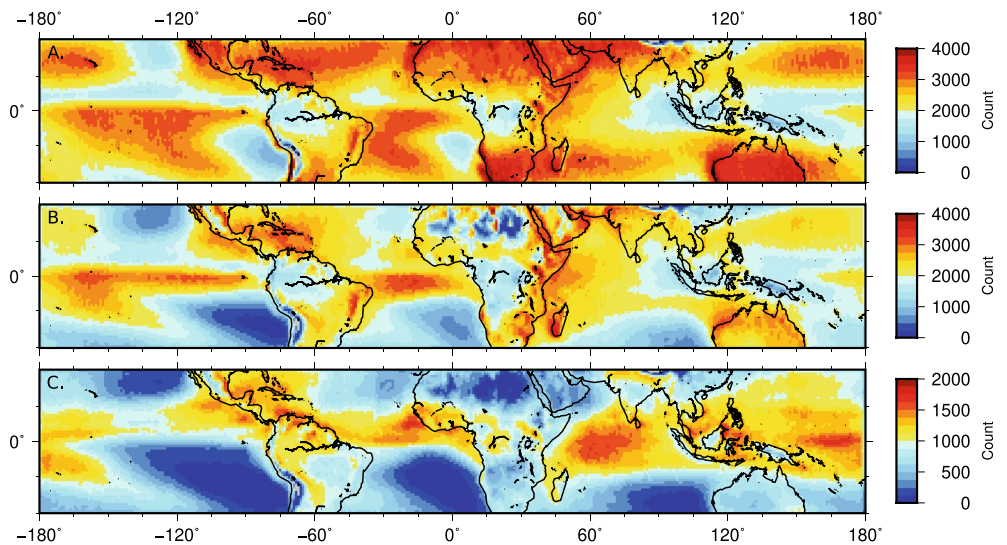


Figure 1. 1×1 degree bin counts of (a) the total number of IASI/MUSICA retrievals prior to QA for the 2015–2020 period; (b) the number of points after the QA selection criteria; (c) the number of points passing QA that are also associated with a value of I_{org} .

Precipitation data are derived from the GPM IMERG Final Precipitation L3 1 day $0.1^\circ \times 0.1^\circ$ V06 (*GPM – 3IMERGDF*) data set (Huffman et al., 2019). Latent heating profiles are from the GPM DPR Spectral Latent Heating Profiles L2 1.5 hr 5 km V07 product (GPM Science Team, 2022). Cloud-top pressure and high-cloud fraction data is from MODIS (Platnick et al., 2003–02). Cloud-top pressures were estimated using the technique of Menzel et al. (2008). The MODIS cloud products are generated for each granule, where a granule consists of 5 min of data. Cloud-top pressures are generated at a 5 km resolution from the average of the cloudy pixel radiances within each 5 km area, using the cloud mask to identify cloudy pixels. High-cloud fractions are defined as the fraction of clouds with cloud-top pressures below 400 hPa. These datasets are interpolated to the time and location of the MUSICA IASI retrievals.

RH profiles are derived from the SAPHIR sounder on the Megha-Tropiques satellite. The SAPHIR sounder is a passive microwave radiometer measuring the upwelling radiation thanks to 6 channels spanning the 183.31 GHz absorption line, yielding RH profiles that describe the atmosphere at six pressure levels between 100 and 950 hPa (Brogniez et al., 2016; Sivira et al., 2015). The nominal footprint size is 10 km at nadir. The satellite samples a given point between 3 and 5 times daily, and here we use daily averages of the operational Level 2 RH product gridded at a $1^\circ \times 1^\circ$ resolution, in which we retain data with at least 95% valid RH values within each gridbox. The SAPHIR RH data is useful as an independent measure of humidity because the retrieval does not rely on a priori assumptions about temperature profiles or integrated water vapor content.

The principal data set used in this study is the global, multi-year MUSICA IASI H_2O and δD data set (Diekmann, Schneider, Ertl, et al., 2021), which is based on radiance measurements from the nadir thermal infrared sensor IASI on board the Metop satellites of EUMETSAT. The satellite ground pixel diameter is 12 km (at nadir), with a full swath width of 2,200 km. The main sensitivity limited to the 2–7 km range. We focus on retrievals centered at 710 hPa, which samples from 870 hPa to 500 hPa (Diekmann, Schneider, Ertl, et al., 2021). We analyze the complete data set from 2015 through 2020, which for the tropical domain ($30^\circ S$ to $30^\circ N$) consists of a total of just over 54 million retrievals (Figure 1a). We then applied the QA criteria recommended by Diekmann, Schneider, Ertl, et al. (2021) and select only those data points with no or little contamination from clouds, fair or good retrieval fit quality, good vertical sensitivity, and with δD error less than 40‰ for a total of over 43 million paired H_2O and δD retrievals (Figure 1b). The I_{org} metric is not defined at every point in the tropics at every time, so the final data set we use in this study consists of just over 17 million H_2O and δD retrievals for which I_{org} is defined (Figures 1c and 2a). Except for very dry conditions, the errors in δD are within 25‰.

Because IASI is an infrared instrument, there are no retrievals for cloudy conditions, and there may thus be a concomitant dry bias in the data. Biases in isotopic measurements are challenging to quantify, but clear-sky

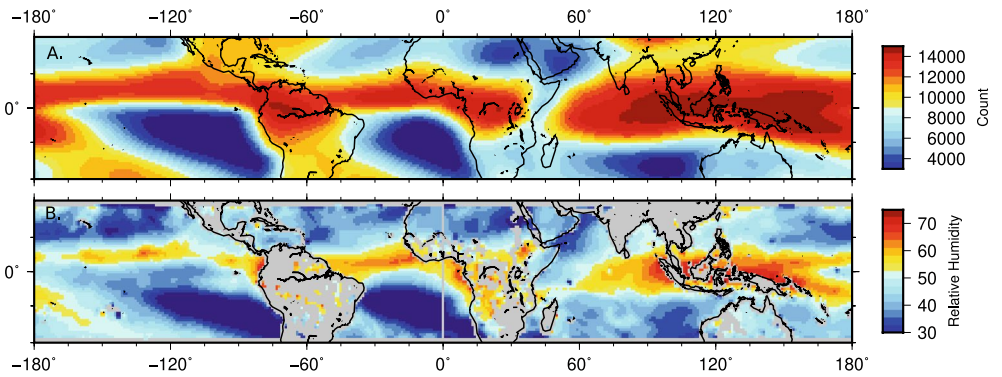


Figure 2. 1×1 degree (a) bin counts of I_{org} values for the 2015–2020 period; (b) bin-averages of SAPHIR Relative humidity (RH) from the 700–550 hPa level for the 2015–2020 period. Note the correspondence between regions of low RH and the points removed by the IASI/MUSICA QA criteria in Figure 1.

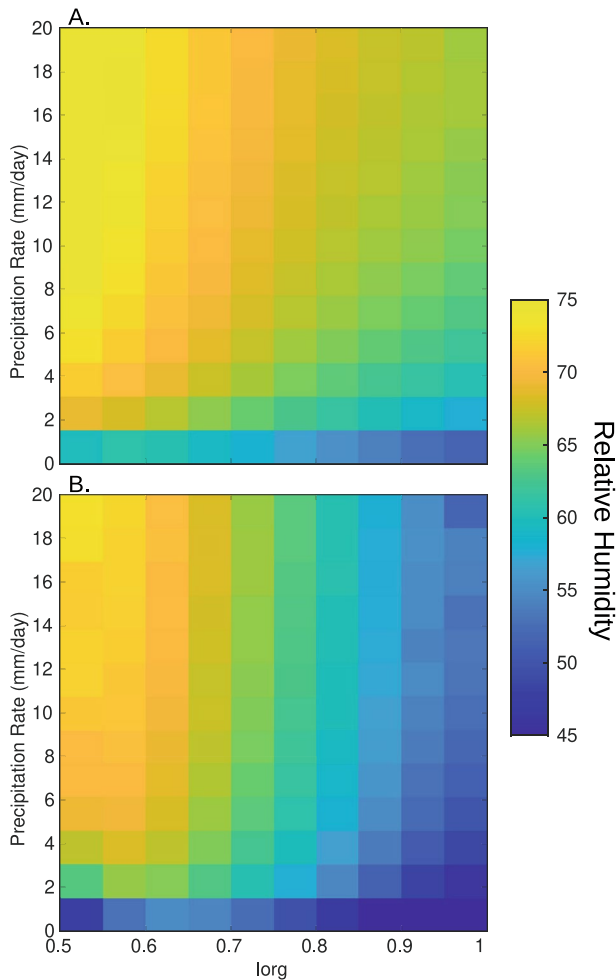


Figure 3. (a) SAPHIR Relative humidity (RH) from the 700–550 hPa level; (b) RH computed from IASI mixing ratio retrievals and ERA Reanalysis temperatures. While the structure of the I_{org} /precipitation rate relationships is consistent, IASI-derived RH subject to our selection criteria averages about 6.8% below SAPHIR RH, with a maximum difference of 16% for the highest I_{org} and highest precipitation rates and a minimum difference of 2% for I_{org} of around 0.65 and precipitation rates above 5 mm/day.

measurements made near regions of active, deep convection still show super-Rayleigh conditions (Diekmann, 2021; Noone, 2012), suggesting that key in-cloud processes can still influence the isotopic composition of the surrounding air. In IASI, the driest points are rejected (Figure 2b). Therefore, the mean RH for the smallest precipitation rates is overestimated by IASI relative to SAPHIR by up to 16% (Figure 3). While the structure of the I_{org} /precipitation rate relationships is consistent, IASI-derived RH subject to our selection criteria averages about 6.8% below SAPHIR RH, with a maximum difference of 16% for the highest I_{org} and highest precipitation rates and a minimum difference of 2% for I_{org} of around 0.65 and precipitation rates above 5 mm/day. We expect that the mean q retrieved by IASI for the smallest precipitation rates is also overestimated by a maximum of 1 g/kg. The impact of this sampling bias on water isotopologues depends on the relationship between q and δD , which will be shown to depend on organization, but based on the ranges of observed $q - \delta D$ slopes, this impact likely does not exceed about 5‰.

3. Results

3.1. Global Maps

Unless otherwise indicated, we consider low and high I_{org} to correspond to $0.5 < I_{org} < 0.65$ and $I_{org} > 0.8$, respectively. We also divide our analysis into low and high precipitation conditions, corresponding to precipitation rates between 1 mm/day and 2 mm/day and between 5 mm/day and 7 mm/day, respectively. Figure 4 shows the number of data points corresponding to low I_{org} and low precipitation rates (Figure 4a); low I_{org} and high precipitation rates (Figure 4b); high I_{org} and low precipitation rates (Figure 4d); and high I_{org} and high precipitation rates (Figure 4d). Low values of I_{org} occur most frequently over the Maritime Continent, the western Pacific Ocean, and the eastern Indian Ocean, with additional clusters over tropical Central and South America. High values of I_{org} occurs less frequently overall than low I_{org} , but there are regions of higher occurrence in the tropical Pacific, the westernmost Indian Ocean, and over the Caribbean and South America.

Precipitation rates are spatially variable and differ widely for low I_{org} (Figure 5a) and high I_{org} (Figure 5b). Within the Intertropical Convergence Zone and over the Maritime Continent, average rainfall exceeds 12 mm/day for low values of I_{org} , while precipitation rarely exceeds 3 mm/day for high values of I_{org} , with the notable exception of Amazonia. In line with previous

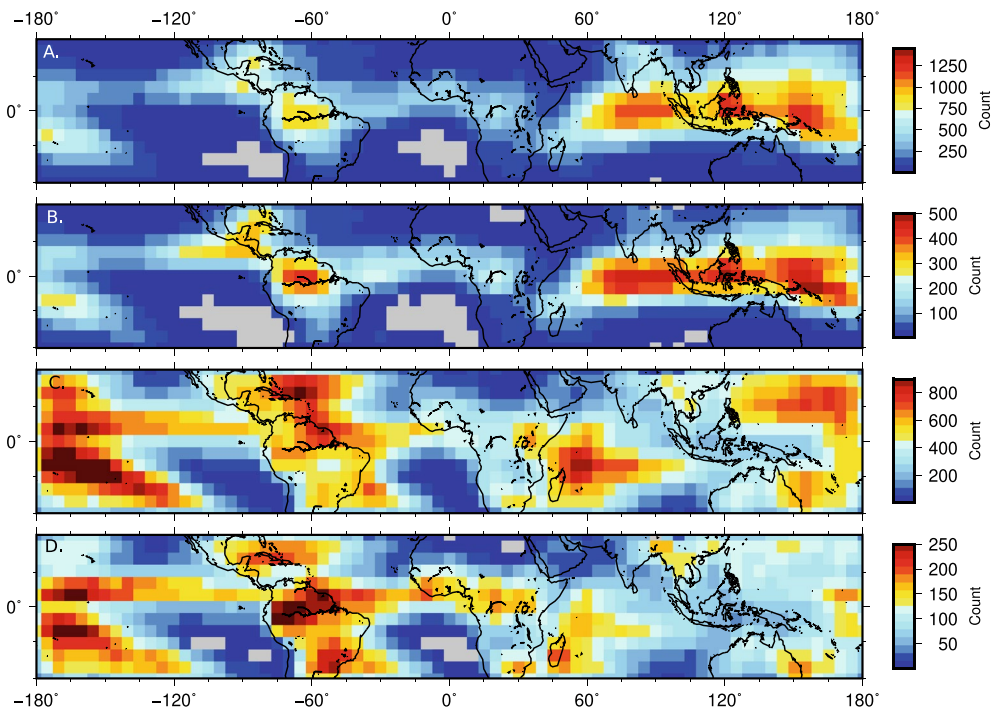


Figure 4. Maps showing the count of data points from 2015 to 2020 in 5×5 degree bins for (a) low I_{org} (between 0.5 and 0.65) and low precipitation rates (between 1 mm/day and 2 mm/day); (b) low I_{org} and high precipitation rates (between 5 mm/day and 7 mm/day); (c) high I_{org} (greater than 0.8) and low precipitation rates; (d) high I_{org} and high precipitation rates. Note the different color scales in each panel. Gray colors indicate no data.

studies (Lacour et al., 2018; Tobin et al., 2012), we will sort the isotopic data by precipitation rate in order to distinguish the impact of convective organization from the impact of convective intensity.

We now investigate the global geographic relationships between I_{org} , mixing ratio, and δD . In Figures 6 and 7, we bin-average all of the 2015–2020 data into $5^\circ \times 5^\circ$ domains and we show the differences in mixing ratio, water vapor δD and D_{rl} between low and high I_{org} for precipitation rates between 1 mm/day and 2 mm/day (Figure 6) and for precipitation rates between 5 mm/day and 7 mm/day (Figure 7). At low precipitation rates (Figure 6), the 710 hPa mixing ratios are generally higher for low I_{org} than for high I_{org} , with a median difference of 0.97 g/kg, with sharper differences over the Maritime Continent, South America, and South Asia reaching as high as 2.59 g/kg over South Asia (Figure 6a). Water vapor δD (Figure 6b) differences at low precipitation rates are generally negative, with a median difference of around -5.8% , but reaching as low as -35% over

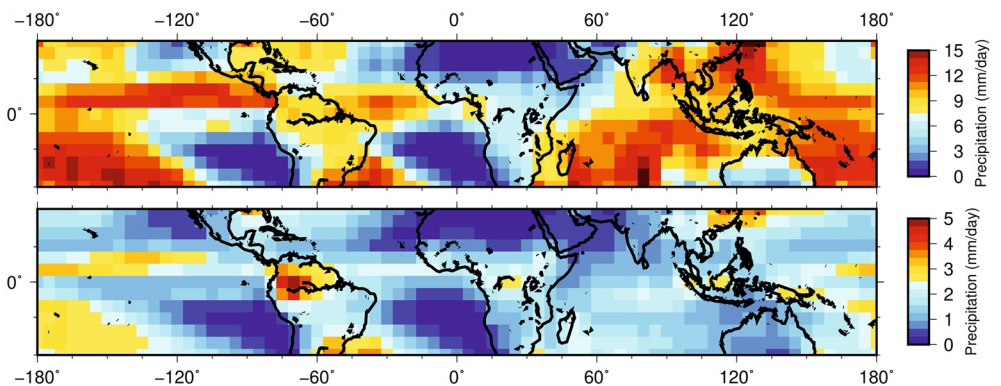


Figure 5. Bin-averaged precipitation rate in mm/day for (a) I_{org} between 0.5 and 0.65 and (b) I_{org} above 0.8. Bin size is 5×5 degrees; note that the color scales are different for the two panels.

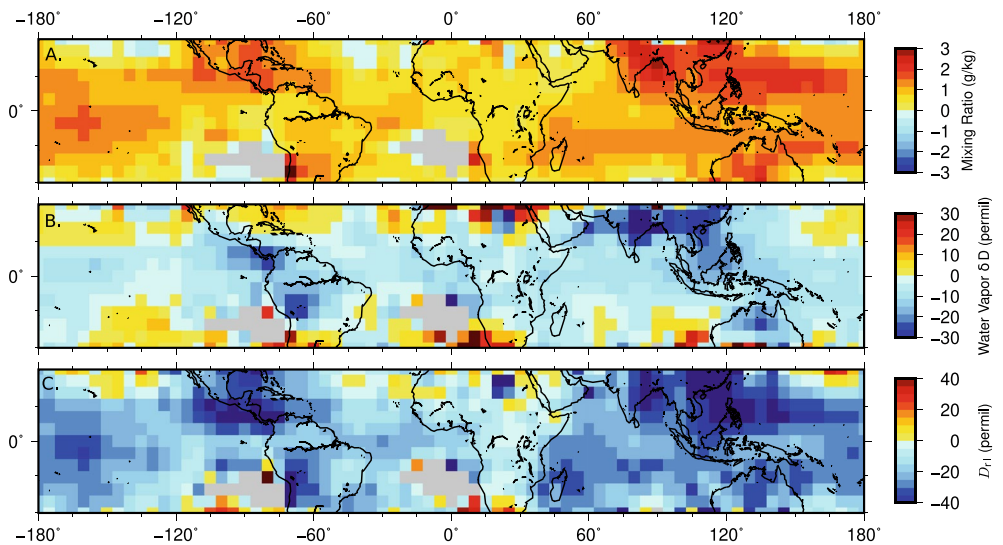


Figure 6. Maps showing the difference between low and high I_{org} at precipitation rates between 1 mm/day and 2 mm/day. (a) Mixing ratio from IASI; (b) water vapor δD ; (c) deviation from Rayleigh distillation.

South Asia and Central and South America. Values of D_{rl} at low precipitation rates and low I_{org} are also generally negative, with a median difference of -22‰ but reaching as low as -62‰ over South Asia and Central America.

At higher precipitation rates, mixing ratio differences (Figure 7a) are slightly higher than at lower precipitation rates, with a median difference of about 1.03 g/kg but reaching as high as 2.75 g/kg over South Asia. δD differences are more negative than for lower precipitation rates, with a median difference of -8.5‰ , but reaching as low as -43‰ , and D_{rl} differences are also more negative at these higher precipitation rates, with a median difference of -25‰ for high precipitation rates, but reaching as low as -66‰ . In general, these results indicate that unaggregated convection moistens and isotopically depletes the atmosphere more than highly aggregated convection, an effect that increases with precipitation rate. The low values of D_{rl} further indicate a prominent role for condensate evaporation in this moistening.

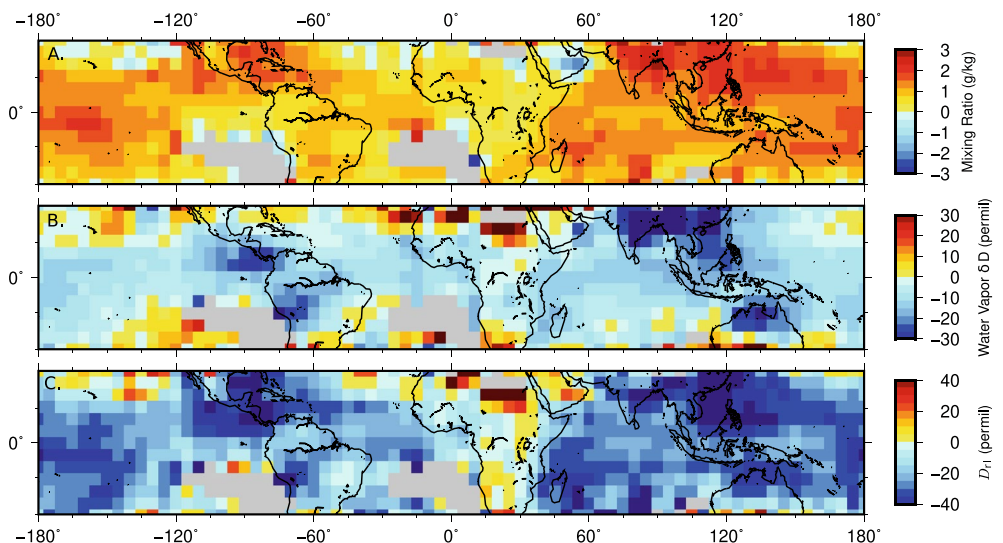


Figure 7. As in Figure 6 for precipitation rates between 5 mm/day and 7 mm/day.

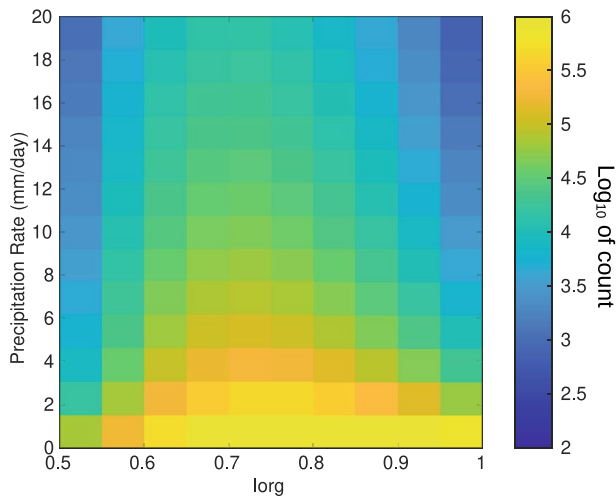


Figure 8. The count of IASI points as a joint function of I_{org} and precipitation rate as the base 10 logarithm of the count. The range of bin counts spans a maximum of 210,000 points to a minimum of 19 points.

3.2. Sorting by Degree of Aggregation and Precipitation Rate

In Figure 9, we bin-average all of the 710 hPa MUSICA IASI isotopic and mixing ratio data by I_{org} and precipitation rates (see Figure 8 for the number of points in each bin). At any given precipitation rate, mixing ratios are higher and δ values are lower for unaggregated convection than for aggregated convection. The mixing ratios (Figure 9a) decrease with increasing I_{org} and decreasing precipitation rate, from around 8 g/kg for unaggregated convection with high precipitation rates to below 4 g/kg for aggregated convection and low precipitation rates. Mixing ratios increase with increasing precipitation rates, but aggregated convection is always associated with drier conditions than unaggregated convection at the same precipitation rate, and the rate of moistening with precipitation rate is greater for low values of I_{org} , an important result that indicates the complex interplay between convection, its degree of aggregation, precipitation efficiency, and environmental moistening. We will visit this issue in more detail in the next section. For I_{org} below 0.65 (Figure 9b), the water vapor δD decreases with increasing precipitation rates from around -180‰ at the lowest precipitation rates to around -195‰ at 20 mm/day. For I_{org} of around 0.75, δ values remain roughly constant at -178‰ , even with increasing precipitation rates. At higher values of I_{org} , the δ values increase with increasing precipitation rates, rising from -180‰ to

over -170‰ at 20 mm/day. D_{rl} is shown Figure 9c and decreases sharply with precipitation rate for I_{org} below 0.6, from -30‰ at the lowest precipitation rates to nearly -100‰ at precipitation rates of 20 mm/day. For higher values of I_{org} , precipitation rates above around 2 mm/day do not significantly affect D_{rl} , but D_{rl} rises from around -65‰ for $I_{org} = 0.7$ to around -25‰ for $I_{org} > 0.95$. These results are consistent with moistening and isotopic depletion of water vapor for weakly aggregated convection and only modest moistening along with isotopic enrichment for more highly-aggregated convection.

A common and convenient way to visualize the co-variability of mixing ratio and isotopic composition is to plot δ values versus their corresponding mixing ratios, and we show three such figures in Figure 10, corresponding, respectively, to low, medium, and high values of I_{org} . In this figure, the mixing ratio and the δD values are bin-averaged by precipitation rate (shown by the colored dots). In all cases, the mixing ratio increases with increasing precipitation rate, but the slope of the $q - \delta$ relationship systematically varies with I_{org} . As initially illustrated in Figure 9, we can more clearly see the negative correlation between q and δD for low values of I_{org} in panel A, how δD is nearly invariant with increasing mixing ratio and precipitation rate for intermediate values of I_{org} in panel B, and the positive correlation between q and δD for high values of I_{org} in panel C. These relationships illustrate how the paradigm of convective aggregation allows us to efficiently discriminate positive and negative $q - \delta D$ correlations that have been previously reported (Diekmann, Schneider, Knippertz, et al., 2021; Lacour et al., 2018).

3.3. Processes Governing I_{org} -Precipitation Rate- δD Relationships

Now that we have established that there is indeed a systematic relationship between convective aggregation and the isotopic composition of water vapor, we seek to understand the suite of processes that govern these relationships. Figure 11 shows profiles of ERA vertical velocity for precipitation rates between 1 mm/day and 2 mm/day (ω , in panel A) and for precipitation rates between 5 mm/day and 7 mm/day (Figure 11b). Regardless of precipitation rate, the strongest ascent is associated with I_{org} below 0.6 and above 350 hPa, with ascent in excess of -95 hPa/day for precipitation rates between 5 mm/day and 7 mm/day, and at the lowest values of I_{org} . The strongest subsidence is associated with low precipitation rates at I_{org} above 0.9 and is centered at around 400 hPa. For low precipitation rates, the transition between ascent and subsidence occurs between I_{org} values of 0.7 and 0.8, while for higher precipitation rates, subsidence is restricted to regions above 400 hPa and I_{org} above 0.9.

There is a reasonably close association between the vertical velocities shown in Figure 11 and the RH shown in Figure 12. The highest RH, about 70% is found between 800 hPa and 900 hPa for I_{org} below 0.6 and precipitation rates between 5 mm/day and 7 mm/day, with a relatively sharp transition to lower RH at around 500 hPa. The lowest RH, below around 20% is associated with strong subsidence above 400 hPa and I_{org} above around

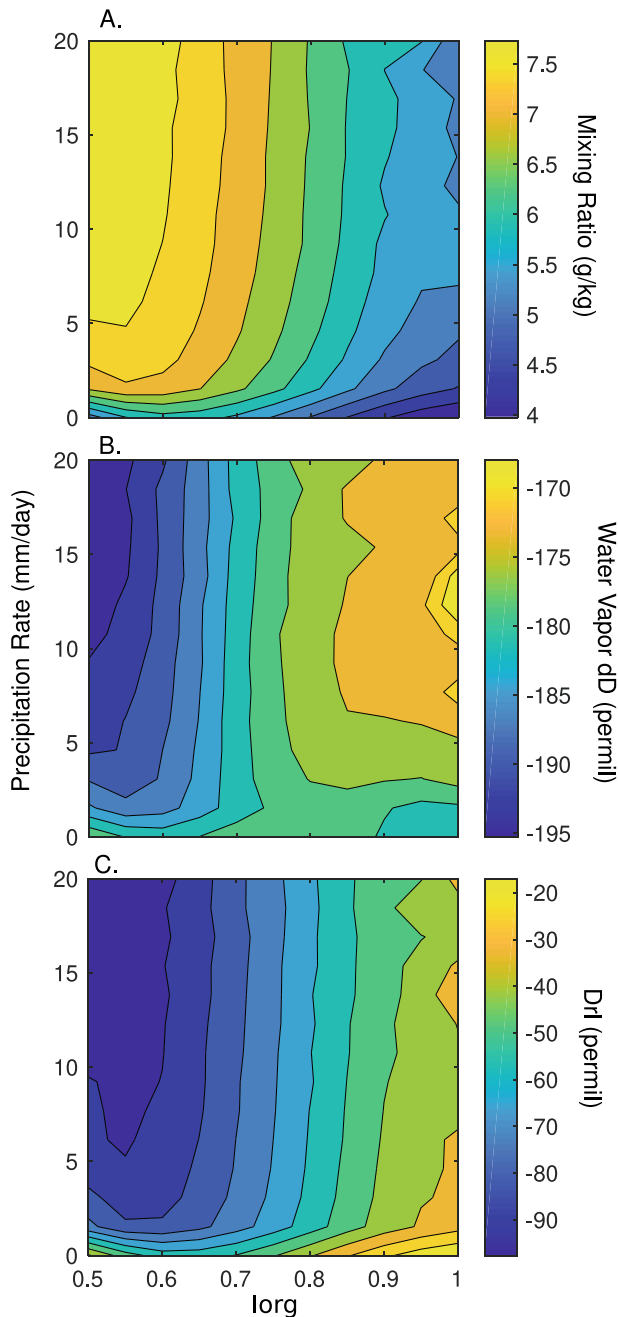


Figure 9. Bin-averaged (a) mixing ratio, (b) water vapor δD (permil), and (c) D_{RL} as a joint function of I_{org} and precipitation rate (mm/day). All data are from the 710 hPa level.

0.9. The deep layer of humid air at low I_{org} is consistent with the observed anti-correlation between moistening and isotopic composition. As shown by Lawrence et al. (2004) and Lee and Fung (2008), partial evaporation of condensate from deep convection in a relatively moist atmosphere can lead to an isotopic depletion with increasing precipitation rates.

The impact of precipitation rate on the top-heaviness of the vertical velocity profiles as a function of I_{org} is shown in Figure 13. The difference in ω between the 920 hPa and 300 hPa levels sharply increases with precipitation rate for the lowest values of I_{org} , representing an increase in top-heaviness with increasing precipitation rate, but this effect decreases with increasing values of I_{org} . Above I_{org} of around 0.75, the profiles become bottom-heavy, with increasing bottom-heaviness at higher values of I_{org} regardless of precipitation rate.

The dependence of convective depth and intensity on I_{org} and precipitation rate are further illustrated in Figure 14. Figure 14a shows how the high cloud fraction decreases with increasing I_{org} for a given precipitation rate; for example, at a precipitation rate of 10 mm/day, the high cloud fraction decreases from 0.8 for I_{org} of 0.5 to 0.5 at I_{org} of 1. Figure 14b shows how cloud top pressure increases with increasing I_{org} for a given precipitation rate. At a precipitation rate of 10 mm/day, the cloud top pressure increases from 410 hPa for I_{org} below 0.6 to 650 hPa for the highest values of I_{org} . Finally, Figure 14c shows the sharp decrease in the altitude of maximum latent heating with increasing I_{org} ; again focusing on a precipitation rate of 10 mm/day, we see that the altitude of maximum latent heating decreases from 5.2 km for low values of I_{org} to just over 4 km for the highest values of I_{org} . From this data, it appears that the maximum in δD seen in Figure 9 occurs for aggregated convection ($I_{org} > 0.8$) above precipitation rates of 5 mm/day when the altitude of maximum latent heating rises above the IASI observation level of 710 hPa, suggesting that the maximum δD in this data set may be related to outflow of convection near the level of observation. The patterns of humidity variations with I_{org} and precipitation rate in Figure 9 are very similar to those of cloud top pressure (Figure 10b). The rate of moistening is greater for low values of I_{org} , as is the rate of decrease of cloud top pressure. This is because strongly aggregated conditions with very low precipitation rate are typically associated with shallow convection that does not reach the 710 hPa level, leaving the free troposphere very dry. As soon as the level of convective detrainment exceeds 710 hPa (i.e., corresponding to cloud-top pressure around 600 hPa, Figure 10b), the 710 hPa level is moistened by convection.

Figure 15 summarizes our interpretation of the relationships between aggregation, precipitation rate, and isotopic composition presented above. At low precipitation rates, unaggregated convection ($I_{org} < 0.6$) is associated with modest high-cloud fractions and moderate ascent. Evaporation of the rain in the lower troposphere acts to moisten the troposphere while reducing the water vapor δD to values below a reference Rayleigh distillation curve, yielding D_{rl} values below zero. The low δD values are then propagated through the

entire tropospheric column by convective mixing (Risi et al., 2021). For aggregated convection (I_{org} above 0.8) at low precipitation rates, strong subsidence keeps convective outflow near or below the observation level. At higher precipitation rates, convection at low I_{org} deepens as ascent rates increase, with greater rain evaporation leading to sharply lower values of δD and D_{rl} . For high values of I_{org} and high precipitation rates, water vapor δD reaches its maximum as the altitude of maximum latent heating rises just above the main MUSICA IASI observation level of 710 hPa. We interpret this δD maximum as reflecting convective outflow of isotopically-enriched water vapor. At intermediate values of I_{org} , there is little change in either δD or in D_{rl} regardless of precipitation rate.

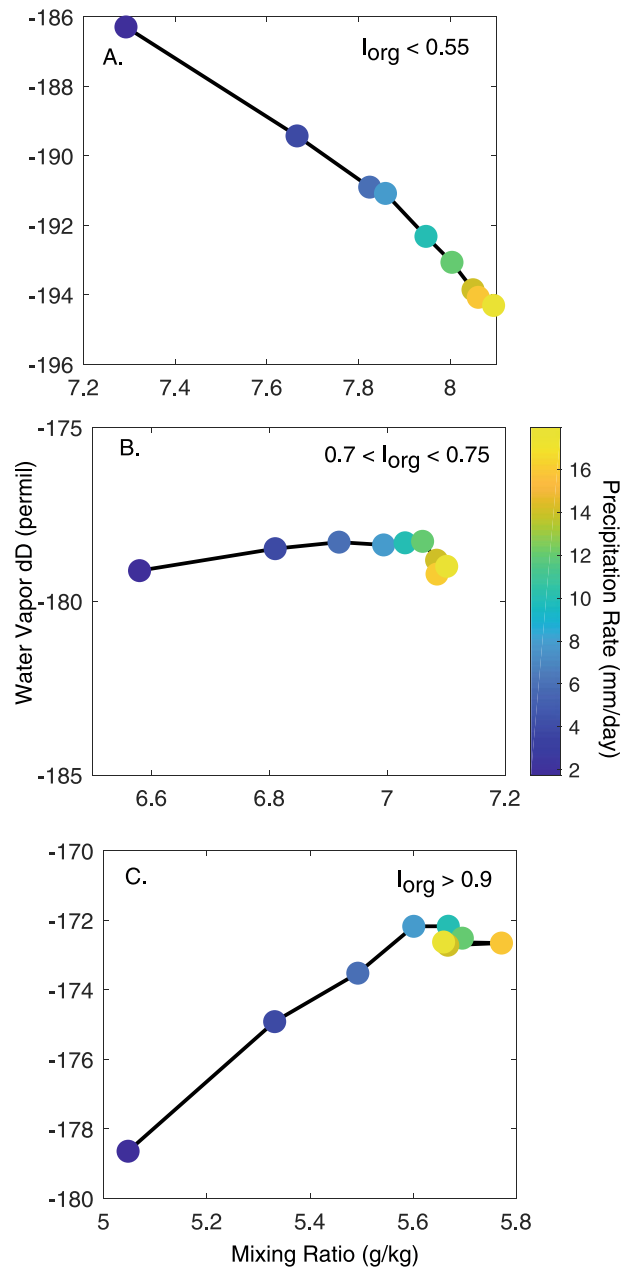


Figure 10. Mixing ratio (q) and δD plotted as bin-averages by increasing precipitation rates for (a) $I_{org} < 0.55$; (b) $0.7 < I_{org} < 0.75$ and (c) $I_{org} > 0.9$. Colored dots indicate the average precipitation rate of each bin. The y-axes in all panels span 10‰ to facilitate comparison.

4. Discussion

Our results illustrate how convective aggregation exerts a significant impact on atmospheric water vapor. For a given precipitation rate, water vapor associated with unaggregated convection with top-heavy vertical velocity profiles is isotopically depleted relative to highly aggregated convection with bottom-heavy vertical velocity profiles, likely owing to a greater degree of condensate evaporation in the unaggregated case. Because the volume of cloud-free air is typically much larger than the volume of cloudy air, satellites are mostly sampling cloud-free air and our results here are of course limited to those clear-sky settings in which satellite retrievals are possible. A valuable complement to the present study, which is focused exclusively on water vapor, would be to extend this analysis to precipitation data. Such a study would provide valuable insight into how these processes

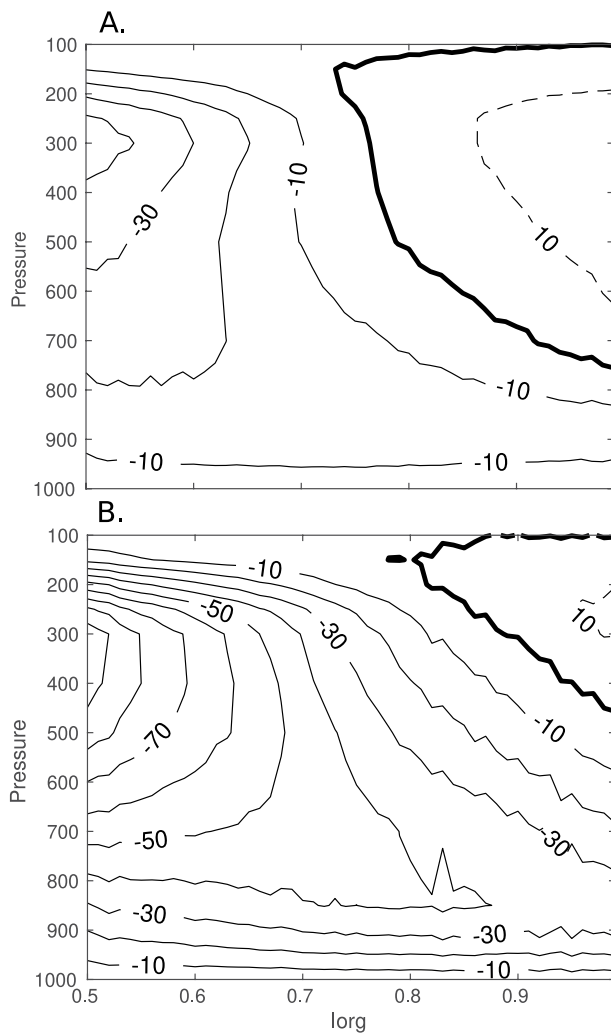


Figure 11. Average vertical profiles of ERA vertical pressure velocity (ω , hPa/day) sorted by I_{org} for precipitation rates (a) between 1 mm/day and 2 mm/day and (b) between 5 mm/day and 7 mm/day.

govern not just the environmental water vapor, but the full suite of condensation and precipitation processes in convection under a variety of aggregated conditions.

Based on a total-column water budget, previous studies have shown that when moisture convergence occurs at higher altitude, the rain is more isotopically depleted (Moore et al., 2014; Torri et al., 2017). A similar argument was made for the vapor by Bailey et al. (2017). Our results are consistent with these studies. Our study further supports the role of rain-vapor exchanges in establishing the total-column water budget equilibrium in which the vapor is more depleted when the moister convergence occurs higher in altitude.

Several studies have found that organized convection in the form of squall lines (Risi et al., 2008; Tremoy et al., 2014), tropical cyclones (Chakraborty et al., 2016; Lawrence et al., 2004; Xu et al., 2019) and mesoscale convective systems (Kurita, 2013) is associated with more depleted water vapor, results that appear to be at odds with the present study. This discrepancy is likely at least partially related to the complicated relationships between convective aggregation and vertical velocity profiles. As was shown here and by Tsai and Mapes (2022), unaggregated convection is, on average, associated with more top-heavy vertical velocity profiles than aggregated convection, but those averages hide the variability in the relationships between aggregation and vertical velocity. For example, several studies have shown that the vertical velocity profiles of tropical cyclones can be top-heavy (Black et al., 1996; Nelson et al., 2019), even though convection is highly aggregated. Similarly, vertical velocity profiles for squall lines and mesoscale convective systems can also be top-heavy, although there is wide variability (Garstang et al., 1994; Houze, 1989). To disentangle the relative impact of aggregation and convective depth, we could redo the present analysis but for a given shape of omega profile (e.g., as in Tobin et al. (2012)). However, given the tight relationship between aggregation and convective depth, sampling becomes an issue. Disentangling the links between aggregation and vertical velocity profiles thus remains an important priority for future research, and the isotopic composition of water vapor may be a valuable tool for such studies.

Our study raises some interesting questions on how convective aggregation may leave an isotopic signal in paleoclimate archives (Holloway et al., 2017).

Several paleoclimate records have been interpreted as indicating the past frequency of organized convective systems (Baldini et al., 2016; Frappier et al., 2007; Maupin et al., 2021; Medina-Elizalde & Rohling, 2012) and in deep-time applications to snowball Earth (Abbot, 2014). The isotopic variations observed in the present study span about 25‰ between unaggregated and aggregated convection. While additional research is needed to exploit our results for paleoclimate applications, this range could plausibly be recorded in suitable proxy records. Furthermore, many paleoclimate studies interpret isotopic records in terms of the isotope amount effect, linking lower δ values to increased precipitation rates in the tropics (Lachniet, 2009), but our results here suggest that changes in convective aggregation could potentially confound such interpretations.

The results of this study may provide observational constraints for modeling studies, with relevance to the issues raised above. Our results from low I_{org} settings are consistent with the modeling study of Risi et al. (2021), who used large eddy simulations and a two-column model to show how water vapor δD values decrease with precipitation rate in unaggregated convection. They showed a close connection between the higher humidity in unaggregated convection and the mechanism for isotopically depleting the atmosphere. When the RH is high in regions of ascent, there is less snow sublimation and a smaller fraction of rain evaporation, with both effects leading to more depleted water vapor. In regions of large scale descent, entrainment of dry air into clouds reduces the vertical isotopic gradient and limits the depletion of tropospheric

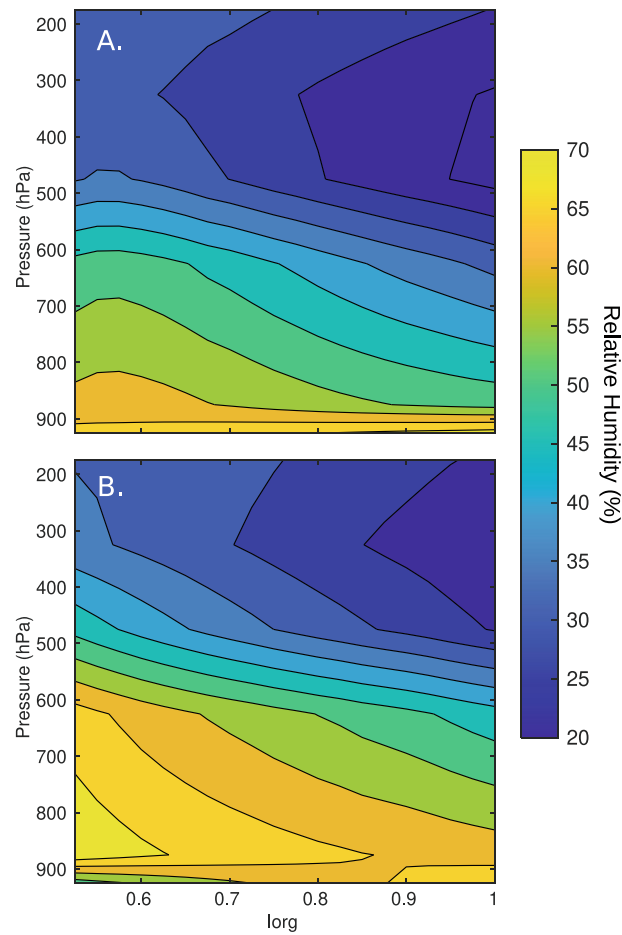


Figure 12. As in 11 for SAPHIR relative humidity.

water vapor. Risi et al. (2021) did not compute D_{rl} , but the increasingly negative values of this parameter with precipitation rate for $I_{org} < 0.6$ would seem to support their conclusions. Risi et al. (2021) focused on unaggregated convection, but we found little change in D_{rl} with increasing precipitation rates for $I_{org} > 0.8$, which is consistent with their results for conditions of large-scale subsidence. Systematic, isotope-enabled modeling studies that sweep through a range of aggregation states and precipitation rates could prove particularly fruitful for better understanding how convective aggregation impacts Earth's climate.

modeling studies that sweep through a range of aggregation states and precipitation rates could prove particularly fruitful for better understanding how convective aggregation impacts Earth's climate.

5. Conclusions

The goal of this study was to use remote sensing datasets of water vapor isotopic composition along with objective measures of convective aggregation to better understand the impact of convective aggregation on atmospheric water vapor. We found that unaggregated convection, with I_{org} below 0.6, is associated with a top-heavy vertical velocity profile and an anticorrelation between mixing ratio and water vapor δD with increasing precipitation rate, consistent with partial hydrometeor evaporation. For I_{org} close to 0.5, water vapor δD values reach a minimum of around -195‰ at a mixing ratio of 8 g/kg and a precipitation rate of 20 mm/day. Highly aggregated convection (I_{org} above 0.8) is associated with a bottom-heavy vertical velocity profile and positive correlation between mixing ratio and δD , a result that is consistent with isotopic enrichment from detrainment of shallow convection near the

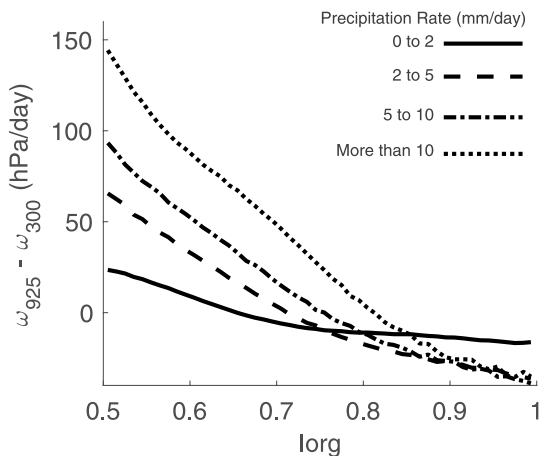


Figure 13. Difference between ω at 925 hPa and at 300 hPa, illustrating links between top-heaviness of convection as a function of I_{org} and precipitation rate. More positive y-axis values indicate a more top-heavy profile.

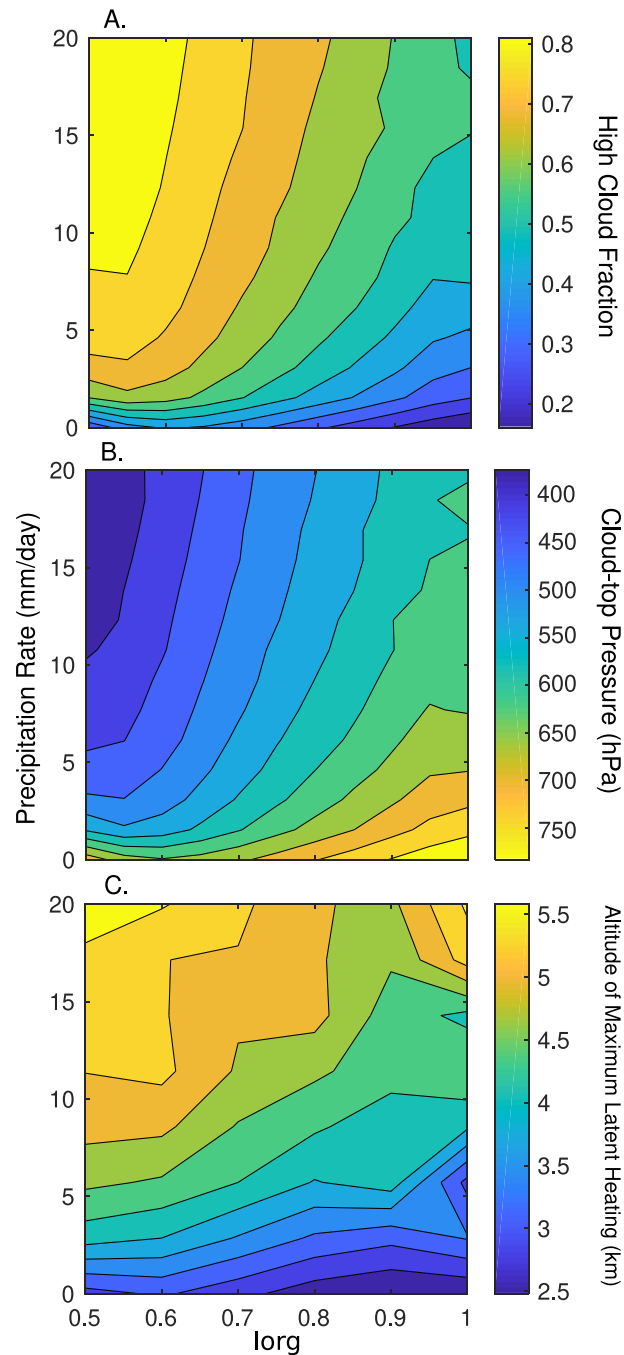


Figure 14. MODIS (a) High cloud fraction (defined as cloud-top pressure <400 hPa); (b) Cloud-top pressure; (c) Altitude of maximum latent heating, all plotted as bin-averaged values of I_{org} versus precipitation rate.

observation level and with mixing of dry air from aloft. For I_{org} above 0.9, δD reaches a value of over -170% at a mixing ratio of 5 g/kg and a precipitation rate of 15 mm/day. Intermediate degrees of aggregation (I_{org} between 0.7 and 0.8) do not display significant variation in δD with mixing ratio or convective intensity, with δD remaining at around -178% regardless of precipitation rate. The results presented here provide a useful framework for better evaluating the links between convective aggregation and water vapor isotopic composition for a range of applications including the interpretation of paleoclimate archives and the evaluation of numerical simulations of convection.

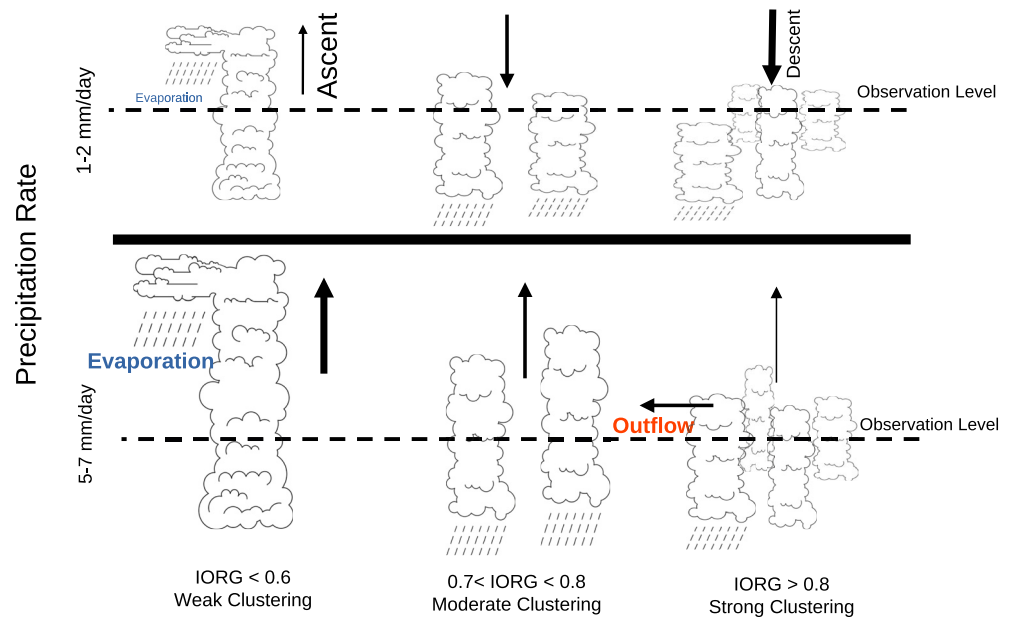


Figure 15. Cartoon summarizing the influence of different aggregation regimes on water vapor isotopic composition as a joint function of I_{org} (horizontal axis) and precipitation rate (vertical axis). Blue (red) colors indicate processes that isotopically deplete (enrich) ambient water vapor. Arrows indicate ascent or descent. Changes in arrow thickness and font size indicate relative changes in strength of the indicated process.

Conflict of Interest

The authors declare no conflicts of interest relevant to this study.

Data Availability Statement

The MUSICA IASI H₂O,delD-pair data set is available at Diekmann, Schneider, and Ertl (2021). The MUSICA IASI full retrieval product (includes among others vertically resolved H₂O profiles) is available at Schneider et al. (2021). The SAPHIR data (Brogniez et al., 2016) is available through the Aeris/ICARE ground segment of Megha-Tropiques (<https://en.aeris-data.fr/projects/megha-tropiques-2/>).

Acknowledgments

This work was supported by the LABEX-IPSL visitor program, the Franco-American Fulbright Foundation, and NSF AGS Grants 1738075 and 1158582 to JG; European Research Council (ERC) under the European Union's Horizon 2020 research program (Grant 694768) to SB and AG. Important developments of the MUSICA IASI processing were made during the project MUSICA (funded by the ERC under the European Community's Seventh Framework Programme (FP7/2007–2013), ERC grant agreement number 256961). The large-scale MUSICA IASI processing was supported by the Deutsche Forschungsgemeinschaft via the projects MOTIV (ID: 290612604) and TEDDY (ID: 416767181). The MUSICA IASI processing was performed on the supercomputer HoreKa funded by the Ministry of Science, Research and the Arts Baden-Württemberg and by the German Federal Ministry of Education and Research. We thank Adriana Bailey and an anonymous reviewer for their insightful comments.

References

- Abbot, D. S. (2014). Resolved snowball Earth clouds. *Journal of Climate*, 27(12), 4391–4402. <https://doi.org/10.1175/jcli-d-13-00738.1>
- Bailey, A., Blossey, P. N., Noone, D., Nusbaumer, J., & Wood, R. (2017). Detecting shifts in tropical moisture imbalances with satellite-derived isotope ratios in water vapor. *Journal of Geophysical Research: Atmospheres*, 122(11), 5763–5779. <https://doi.org/10.1002/2016jd026222>
- Baldini, L. M., Baldini, J. U. L., McElwaine, J. N., Frappier, A. B., Asmerom, Y., Liu, K.-b., et al. (2016). Persistent northward North Atlantic tropical cyclone track migration over the past five centuries. *Scientific Reports*, 6(1), 37522. <https://doi.org/10.1038/srep37522>
- Beucler, T., Leutwyler, D., & Windmiller, J. M. (2020). Quantifying convective aggregation using the tropical moist margin's length. *Journal of Advances in Modeling Earth Systems*, 12(10), e2020MS002092. <https://doi.org/10.1029/2020ms002092>
- Black, M. L., Burpee, R. W., & Marks, F. D. M., Jr. (1996). Vertical motion characteristics of tropical cyclones determined with airborne Doppler radial velocities. *Journal of the Atmospheric Sciences*, 53(13), 1887–1909. [https://doi.org/10.1175/1520-0469\(1996\)053<1887:vmcotc>2.0.co;2](https://doi.org/10.1175/1520-0469(1996)053<1887:vmcotc>2.0.co;2)
- Bony, S., Semie, A., Kramer, R. J., Soden, B., Tompkins, A. M., & Emanuel, K. A. (2020). Observed modulation of the tropical radiation budget by deep convective organization and lower-tropospheric stability. *AGU Advances*, 1(3). <https://doi.org/10.1029/2019av000155>
- Bretherton, C. S., Blossey, P. N., & Khairoutdinov, M. (2005). An energy-balance analysis of deep convective self-aggregation above uniform SST. *Journal of the Atmospheric Sciences*, 62(12), 4273–4292. <https://doi.org/10.1175/jas3614.1>
- Brogniez, H., Fallourd, R., Mallet, C., Sivira, R., & Dufour, C. (2016). Estimating confidence intervals around relative humidity profiles from satellite observations: Application to the SAPHIR sounder. *Journal of Atmospheric and Oceanic Technology*, 33(5), 1005–1022. <https://doi.org/10.1175/jtech-d-15-0237.1>
- Chakraborty, S., Sinha, N., Chattopadhyay, R., Sengupta, S., Mohan, P. M., & Datye, A. (2016). Atmospheric controls on the precipitation isotopes over the Andaman Islands, Bay of Bengal. *Scientific Reports*, 6(1), 19555. <https://doi.org/10.1038/srep19555>
- Coppin, D., & Bony, S. (2015). Physical mechanisms controlling the initiation of convective self-aggregation in a general circulation model. *Journal of Advances in Modeling Earth Systems*, 7(4), 2060–2078. <https://doi.org/10.1002/2015ms000571>
- Craig, H. (1961). Isotopic variations in meteoric waters. *Science*, 133(346), 1702–1703. <https://doi.org/10.1126/science.133.3465.1702>

- Diekmann, C. (2021). Analysis of stable water isotopes in tropospheric moisture during the West African Monsoon. (Unpublished doctoral dissertation).
- Diekmann, C., Schneider, M., & Ertl, B. (2021). MUSICA IASI water isotopologue pair product (a posteriori processing version 2. Institute of meteorology and climate research, atmospheric trace gases and remote sensing (IMK-ASF) [Dataset]. Karlsruhe Institute of Technology (KIT). <https://doi.org/10.35097/415>
- Diekmann, C., Schneider, M., Ertl, B., Hase, F., García, O., Khosrawi, F., et al. (2021). The global and multi-annual MUSICA IASI H₂O, dD pair dataset. *Earth System Science Data*, 13(11), 5273–5292. <https://doi.org/10.5194/essd-13-5273-2021>
- Diekmann, C., Schneider, M., Knippertz, P., Vries, A. J., Pfahl, S., Aemisegger, F., et al. (2021). A Lagrangian perspective on stable water isotopes during the West African monsoon. *Journal of Geophysical Research: Atmospheres*, 126(19), e2021JD034895. <https://doi.org/10.1029/2021jd034895>
- Frappier, A. B., Sahagian, D., Carpenter, S. J., Gonzalez, L. A., & Frappier, B. R. (2007). Stalagmite stable isotope record of recent tropical cyclone events. *Geology*, 35(2), 111–114. <https://doi.org/10.1130/g23145a.1>
- Galewsky, J. (2018a). Relationships between inversion strength, lower-tropospheric moistening, and low-cloud fraction in the subtropical southeast Pacific derived from stable isotopologues of water vapor. *Geophysical Research Letters*, 45(15), 7701–7710. <https://doi.org/10.1029/2018gl078953>
- Galewsky, J. (2018b). Using stable isotopes in water vapor to diagnose relationships between lower-tropospheric stability, mixing, and low-cloud cover near the Island of Hawaii. *Geophysical Research Letters*, 45(1), 297–305. <https://doi.org/10.1002/2017gl075770>
- Galewsky, J., & Hurley, J. V. (2010). An advection-condensation model for subtropical water vapor isotopic ratios. *Journal of Geophysical Research*, 115(D16), D16116. <https://doi.org/10.1029/2009jd013651>
- Galewsky, J., Larsen, H. C. S., Field, R. D., Worden, J., Risi, C., & Schneider, M. (2016). Stable isotopes in atmospheric water vapor and applications to the hydrologic cycle. *Reviews of Geophysics*, 54(4), 809–865. <https://doi.org/10.1002/2015rg000512>
- Garstang, M., Jr., Halverson, J., Greco, S., & Scala, J. (1994). Amazon coastal squall lines. Part I: Structure and kinematics. *Monthly Weather Review*, 122(4), 608–622. [https://doi.org/10.1175/1520-0493\(1994\)122<0608:acslpi>2.0.co;2](https://doi.org/10.1175/1520-0493(1994)122<0608:acslpi>2.0.co;2)
- GPM Science Team. (2022). GPM DPR spectral latent heating profiles L2 1.5 hours 5 km V07, Greenbelt, MD, USA, Goddard Earth Sciences Data and Information Services Center (GES DISC). <https://doi.org/10.5067/GPM/DPR/SLH/2H/07>
- Held, I. M., Hemler, R. S., & Ramaswamy, V. (1993). Radiative-convective equilibrium with explicit two-dimensional moist convection. *Journal of the Atmospheric Sciences*, 50(23), 3909–3927. [https://doi.org/10.1175/1520-0469\(1993\)050<3909:rccwet>2.0.co;2](https://doi.org/10.1175/1520-0469(1993)050<3909:rccwet>2.0.co;2)
- Holloway, C. E., Wing, A. A., Bony, S., Muller, C., Masunaga, H., L'Ecuyer, T. S., et al. (2017). Observing convective aggregation. *Surveys in Geophysics*, 38(6), 1199–1236. <https://doi.org/10.1007/s10712-017-9419-1>
- Houze, R. A. (1989). Observed structure of mesoscale convective systems and implications for large-scale heating. *Quarterly Journal of the Royal Meteorological Society*, 115(487), 425–461. <https://doi.org/10.1002/qj.49711548702>
- Huffman, Stocker, E., Bolvin, D., Nelkin, E., & Tan, J. (2019). GPM IMERG final precipitation L3 1 day 0.1 degree x 0.1 degree V06. <https://doi.org/10.5067/GPM/IMERGDF/DAY/06>
- Hurley, J. V., Verlinden, K. L., Blossey, P. N., Kuang, Z., & Noone, D. (2019). Moist entropy and water isotopologues in a zonal overturning circulation framework of the Madden-Julian Oscillation. *Journal of Geophysical Research: Atmospheres*, 124(3), 1248–1265. <https://doi.org/10.1029/2018jd029510>
- Jin, D., Oreopoulos, L., Lee, D., Tan, J., & Kim, K. (2022). A new organization metric for synoptic scale tropical convective aggregation. *Journal of Geophysical Research: Atmospheres*, 127(13), e2022JD036665. <https://doi.org/10.1029/2022jd036665>
- Kadoya, T., & Masunaga, H. (2018). New observational metrics of convective self-aggregation: Methodology and a case study. *Journal of the Meteorological Society of Japan. Series II*, 96(6), 535–548. <https://doi.org/10.2151/jmsj.2018-054>
- Knapp, K. R., Ansari, S., Bain, C. L., Bourassa, M. A., Dickinson, M. J., Funk, C., et al. (2011). Globally gridded satellite observations for climate studies. *Bulletin of the American Meteorological Society*, 92(7), 893–907. <https://doi.org/10.1175/2011bams3039.1>
- Kurita, N. (2013). Water isotopic variability in response to mesoscale convective system over the tropical ocean. *Journal of Geophysical Research: Atmospheres*, 118(18), 10376–10390. <https://doi.org/10.1002/jgrd.50754>
- Lachniet, M. S. (2009). Climatic and environmental controls on speleothem oxygen-isotope values. *Quaternary Science Reviews*, 28(5–6), 412–432. <https://doi.org/10.1016/j.quascirev.2008.10.021>
- Lacour, J.-L., Risi, C., Worden, J., Clerboux, C., & Coheur, P.-F. (2018). Importance of depth and intensity of convection on the isotopic composition of water vapor as seen from IASI and TES δD observations. *Earth and Planetary Science Letters*, 481, 387–394. <https://doi.org/10.1016/j.epsl.2017.10.048>
- Lawrence, J. R., Gedzelman, S. D., Dexheimer, D., Cho, H. K., Carrie, G. D., Gasparini, R., et al. (2004). Stable isotopic composition of water vapor in the tropics. *Journal of Geophysical Research*, 109(D6), D06115. <https://doi.org/10.1029/2003jd004046>
- Lee, J.-E., & Fung, I. (2008). Amount effect" of water isotopes and quantitative analysis of post-condensation processes. *Hydrological Processes*, 22(1), 1–8. <https://doi.org/10.1002/hyp.6637>
- Maupin, C. R., Roark, E. B., Thirumalai, K., Shen, C.-C., Schumacher, C., Kampen-Lewis, S. V., et al. (2021). Abrupt Southern Great Plains thunderstorm shifts linked to glacial climate variability. *Nature Geoscience*, 14(6), 396–401. <https://doi.org/10.1038/s41561-021-00729-w>
- Medina-Elizalde, M., & Rohling, E. J. (2012). Collapse of classic Maya civilization related to modest reduction in precipitation. *Science*, 335(6071), 956–959. <https://doi.org/10.1126/science.1216629>
- Menzel, W. P., Frey, R. A., Zhang, H., Wylie, D. P., Moeller, C. C., Holz, R. E., et al. (2008). MODIS global cloud-top pressure and amount estimation: Algorithm description and results. *Journal of Applied Meteorology and Climatology*, 47(4), 1175–1198. <https://doi.org/10.1175/2007jamc1705.1>
- Merlivat, L., & Jouzel, J. (1979). Global climatic interpretation of the deuterium-oxygen 18 relationship for precipitation. *Journal of Geophysical Research*, 84(C8), 5029–5033. <https://doi.org/10.1029/jc084ic08p05029>
- Moore, M., Kuang, Z., & Blossey, P. N. (2014). A moisture budget perspective of the amount effect. *Geophysical Research Letters*, 41(4), 1329–1335. <https://doi.org/10.1002/2013gl058302>
- Muller, C. J., & Held, I. M. (2012). Detailed investigation of the self-aggregation of convection in cloud-resolving simulations. *Journal of the Atmospheric Sciences*, 69(8), 2551–2565. <https://doi.org/10.1175/jas-d-11-0257.1>
- Nelson, T. C., Harrison, L., & Corbosiero, K. L. (2019). Examination of the expendable digital dropsonde-derived vertical velocities from the tropical cyclone intensity (TCI) experiment. *Monthly Weather Review*, 147(7), 2367–2386. <https://doi.org/10.1175/mwr-d-18-0414.1>
- Noone, D. (2012). Pairing measurements of the water vapor isotope ratio with humidity to deduce atmospheric moistening and dehydration in the tropical midtroposphere. *Journal of Climate*, 25(13), 4476–4494. <https://doi.org/10.1175/jcli-d-11-00582.1>
- Platnick, S., King, M. D., Ackerman, S. A., Menzel, W. P., Baum, B. A., Riedi, J. C., & Frey, R. A. (2003-02). The MODIS cloud products: Algorithms and examples from terra. *IEEE Transactions on Geoscience and Remote Sensing*, 41(2), 459–473. <https://doi.org/10.1109/tgrs.2002.808301>

- Risi, C., Bony, S., Vimeux, F., Descroix, L., Ibrahim, B., Lebreton, E., et al. (2008). What controls the isotopic composition of the African monsoon precipitation? Insights from event-based precipitation collected during the 2006 AMMA field campaign. *Geophysical Research Letters*, *35*(24), L24808. <https://doi.org/10.1029/2008gl035920>
- Risi, C., Galewsky, J., Reverdin, G., & Briant, F. (2019). Controls on the water vapor isotopic composition near the surface of tropical oceans and role of boundary layer mixing processes. *Atmospheric Chemistry and Physics*, *19*(19), 12235–12260. <https://doi.org/10.5194/acp-19-12235-2019>
- Risi, C., Muller, C., & Blosssey, P. (2021). Rain evaporation, snow melt, and entrainment at the heart of water vapor isotopic variations in the tropical troposphere, according to large-eddy simulations and a two-column model. *Journal of Advances in Modeling Earth Systems*, *13*(4), e2020MS002381. <https://doi.org/10.1029/2020ms002381>
- Samuels-Crow, K. E., Galewsky, J., Sharp, Z. D., & Dennis, K. J. (2014). Deuterium excess in subtropical free troposphere water vapor: Continuous measurements from the Chajnantor Plateau, northern Chile. *Geophysical Research Letters*, *41*(23), 8652–8659. <https://doi.org/10.1002/2014gl062302>
- Schneider, M., Ertl, B., & Diekmann, C. (2021). MUSICA IASI full retrieval product standard output (processing version 3.2.1) [Dataset]. Karlsruhe Institute of Technology (KIT). <https://doi.org/10.35097/408>
- Semie, A. G., & Bony, S. (2020). Relationship between precipitation extremes and convective organization inferred from satellite observations. *Geophysical Research Letters*, *47*(9), e2019GL086927. <https://doi.org/10.1029/2019gl086927>
- Sivira, R. G., Brogniez, H., Mallet, C., & Oussar, Y. (2015). A layer-averaged relative humidity profile retrieval for microwave observations: Design and results for the Megha-Tropiques payload. *Atmospheric Measurement Techniques*, *8*(3), 1055–1071. <https://doi.org/10.5194/amt-8-1055-2015>
- Tobin, I., Roca, R., Tobin, I., Bony, S., & Roca, R. (2012). Observational evidence for relationships between the degree of aggregation of deep convection, water vapor, surface fluxes, and Radiation (Vol. 25, pp. 6885–6904). <https://doi.org/10.1175/jcli-d-11-00258.1>
- Tompkins, A. M., & Semie, A. G. (2017). Organization of tropical convection in low vertical wind shears: Role of updraft entrainment. *Journal of Advances in Modeling Earth Systems*, *9*(2), 1046–1068. <https://doi.org/10.1002/2016ms000802>
- Torri, G., Ma, D., & Kuang, Z. (2017). Stable water isotopes and large-scale vertical motions in the tropics. *Journal of Geophysical Research: Atmospheres*, *122*(7), 3703–3717. <https://doi.org/10.1002/2016jd026154>
- Tremoy, G., Vimeux, F., Soumana, S., Souley, I., Risi, C., Favreau, G., & Oi, M. (2014). Clustering mesoscale convective systems with laser-based water vapor delta O-18 monitoring in Niamey (Niger). *Journal of Geophysical Research-Atmospheres*, *119*(9), 5079–5103. <https://doi.org/10.1002/2013jd020968>
- Tsai, W.-M., & Mapes, B. E. (2022). Evidence of aggregation dependence of 5°-scale tropical convective evolution using a gross moist stability framework. *Journal of the Atmospheric Sciences*, *79*(5), 1385–1404. <https://doi.org/10.1175/jas-d-21-0253.1>
- White, B., Buchanan, A., Birch, C., Stier, P., & Pearson, K. (2017). Quantifying the effects of horizontal grid length and parameterised convection on the degree of convective organization using a metric of the potential for convective interaction. *Journal of the Atmospheric Sciences*, *75*(2), 425–450. <https://doi.org/10.1175/jas-d-16-0307.1>
- Wing, A. A., Emanuel, K., Holloway, C. E., & Muller, C. (2017). Convective self-aggregation in numerical simulations: A review. *Surveys in Geophysics*, *38*(6), 1173–1197. <https://doi.org/10.1007/s10712-017-9408-4>
- Wing, A. A., & Emanuel, K. A. (2014). Physical mechanisms controlling self-aggregation of convection in idealized numerical modeling simulations. *Journal of Advances in Modeling Earth Systems*, *6*(1), 59–74. <https://doi.org/10.1002/2013ms000269>
- Worden, J., Noone, D., Bowman, K., contributors, The Tropospheric Emission Spectrometer science team and data, Beer, R., Eldering, A., & Worden, H. (2007). Importance of rain evaporation and continental convection in the tropical water cycle. *Nature*, *445*(7127), 528–532. <https://doi.org/10.1038/nature05508>
- Xu, T., Sun, X., Hong, H., Wang, X., Cui, M., Lei, G., et al. (2019). Stable isotope ratios of typhoon rains in Fuzhou, Southeast China, during 2013–2017. *Journal of Hydrology*, *570*, 445–453. <https://doi.org/10.1016/j.jhydrol.2019.01.017>